HHS Public Access

Author manuscript

Chem. Author manuscript; available in PMC 2024 May 10.

Published in final edited form as:

Chem. 2024 February 08; 10(2): 713–729. doi:10.1016/j.chempr.2023.11.016.

Influence of structural moieties in squaraine dyes on optoacoustic signal shape and intensity

William M. MacCuaig[1,2], **Carly Wickizer**[3], **Richard S. Van**[3], **Emmanuel R. Buabeng**[4], **Megan R. Lerner**[5], **William E. Grizzle**[6], **Yihan Shao**[3], **Maged Henary**[4,7,*], **Lacey R. McNally**[1,5,8,*]

[1]Stephenson Cancer Center, University of Oklahoma, Oklahoma City, OK 73104, USA

[2]Department of Biomedical Engineering, University of Oklahoma, Norman, OK 73019, USA

[3]Department of Chemistry and Biochemistry, University of Oklahoma, Norman, OK 73019, USA

[4]Department of Chemistry, Georgia State University, Atlanta, GA 30303, USA

[5]Department of Surgery, University of Oklahoma, Oklahoma City, OK 73104, USA

[6]Department of Pathology, University of Alabama at Birmingham, Birmingham, AL 35294, USA

[7]Center for Diagnostics and Therapeutics, Georgia State University, Atlanta, GA 30303, USA

[8]Lead contact

SUMMARY

Optoacoustic imaging has grown in clinical relevance due to inherent advantages in sensitivity, resolution, and imaging depth, but the development of contrast agents is lacking. This study assesses the influence of structural features of squaraine dyes on optoacoustic activity through computational models, *in vitro* testing, and *in vivo* experimentation. The squaraine scaffold was decorated with halogens and side-chain extensions. Extension of side chains and heavy halogenation of squaraines both increased optoacoustic signals individually, although they had a more significant effect in tandem. Density functional theory models suggest that the origin of the increased optoacoustic signal is the increase in transition dipole moment and vibrational entropy, which manifested as increased absorbance in near-infrared region (NIR) wavelengths and decreased fluorescence quantum yield. This study provides insight into the structure-function relationships that will lead guiding principles for optimizing optoacoustic contrast agents. Further

*Correspondence: mhenary1@gsu.edu (M.H.), lacey_mcnally@hotmail.com (L.R.M.).

AUTHOR CONTRIBUTIONS

W.M.M. and L.R.M. designed the project and experiments. M.H. and E.R.B. designed and synthesized the squaraine and cyanine compounds, respectively. C.W., R.S.V., and Y.S. performed computational modeling and analysis. W.M.M. performed *in vitro*, *in vivo*, and ex vivo experimentation. M.R.L. stained and acquired histological images. M.R.L., W.E.G., and L.R.M. evaluated histological images. L.R.M. performed statistical analysis. W.M.M., C.W., R.S.V., and M.H. wrote the draft of the manuscript, and all authors provided comments and edits. L.R.M. and M.H. are the corresponding authors. L.R.M. is the lead contact.

SUPPLEMENTAL INFORMATION

Supplemental information can be found online at https://doi.org/10.1016/j.chempr.2023.11.016.

DECLARATION OF INTERESTS

The authors declare no competing interests.

INCLUSION AND DIVERSITY

We support inclusive, diverse, and equitable conduct of research. One or more of the authors of this paper self-identifies as a gender minority in their field of research.

developments of squaraines and other agents will further increase the relevance of optoacoustic imaging in a clinical setting.

Graphical Abstract

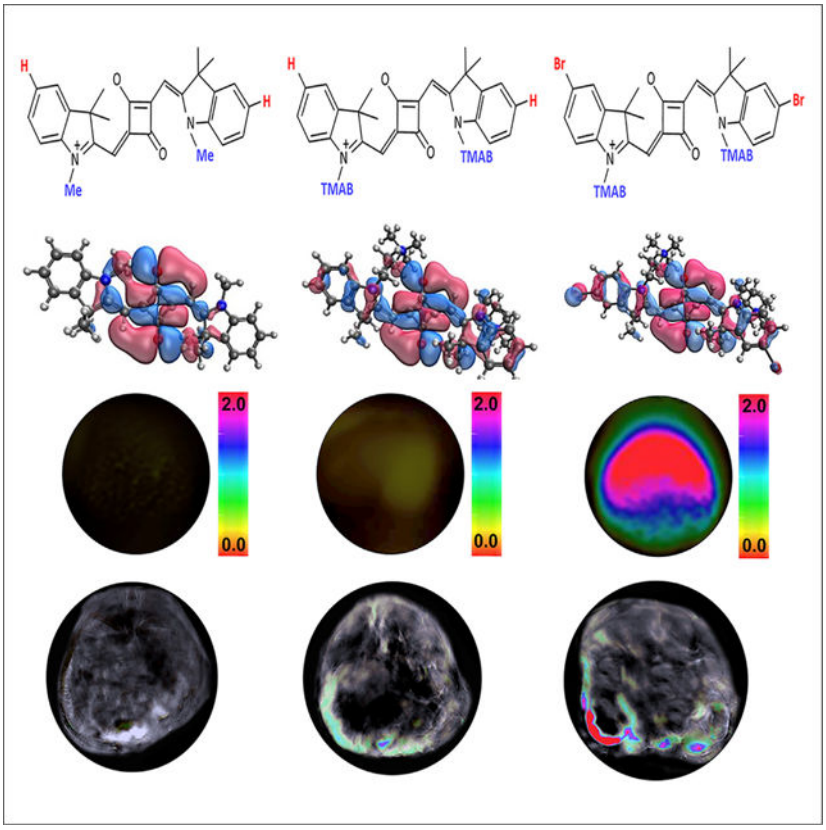

Optoacoustic imaging has grown in clinical relevance due to inherent advantages, but the development of contrast agents is needed for full translational potential. This study assesses the influence of structure of squaraine dyes on optoacoustic activity. Extending side chains and heavy halogenation of squaraines increased optoacoustic signals individually and additively together. This study provides insight that will lead to principles for optimizing optoacoustic agents. Further developments may lead to increased relevance of optoacoustic imaging in a clinical setting.

INTRODUCTION

Optoacoustic imaging is an emerging imaging modality that utilizes the photoacoustic effect to achieve clinically significant resolution at depths beyond current techniques.[1,2] Following unique absorption of near-infrared light by selected optoacoustic agents, thermoelastic expansions generate detectable ultrasonic waves.[3,4] In contrast to optical imaging, optoacoustic imaging overcomes the restriction of depth due to photon scattering while maintaining high sensitivity and spatial resolution on the scale of 10 cells, or 200 μm in a clinical setting, and as low as 75 μm.[1,5,6] This advantage has established optoacoustic imaging as a powerful modality and supports ensuing clinical trials.[1,7–10] Multi-wavelength illumination and processing equipped with optoacoustic tomography,

coined as multispectral optoacoustic tomography (MSOT), allows for separation of optoacoustically active chromophores, including oxyhemoglobin and deoxyhemoglobin, with the caveat that absorption spectra are unique. However, with few distinct endogenous contrast agents,[11,12] MSOT clinical trials have largely been limited to conditions involving differential oxygenation, such as breast cancer,[13–15] inflammatory bowel diseases,[16–18] or dermatologic conditions.[19,20] Utilization of exogenous contrast agents presents an opportunity for optoacoustic imaging to expand in relevancy in the clinic. Optoacoustic imaging has largely exploited commercially available near-infrared dyes, including IR-800-CW,[21,22] indocyanine green (ICG),[23,24] or methylene blue (MB).[25,26] IR-800-CW was specifically engineered for maximum fluorescent signal resulting in sub-optimal optoacoustic signals, or non-unique and non-separable spectral shapes. However, not all near-infrared dyes used for fluorescence present measurable optoacoustic signal, including rhodamine 800.[25]

Although optoacoustic imaging often detects near-infrared fluorescent dyes, the fundamental understanding of structural features that give rise to optoacoustic signal is limited.[25] Generally, the relationship between optoacoustic signal generation and structural features is based upon knowledge from fluorescence and therefore lacks guiding principles for the design of optimized optoacoustic agents. For example, compounds with high ring density, electron-donating groups, and rigidity of the central ring tend to show fluorescent properties.[27,28] However, the generation of fluorescence and optoacoustic signal are different pathways of energy dissipation following absorption of light, therefore, fluorescence quantum yield and optoacoustic activity are inversely related. Because fluorescence is a result of radiative decay and optoacoustic activity is due to non-radiative decay, e.g., generation of heat, it is likely that there are moieties that result in increased optoacoustic activity at the expense of fluorescence. Rhodamine 800, as an opposite example, generates substantial fluorescent signal but no measurable optoacoustic signal.[25]

Squaraine dyes are relatively basic and stable molecules[29] that, in turn, may facilitate a greater understanding of specific influences of structural features on optoacoustic signals. Easily controllable molecules are critical for understanding the origin of complex energy transfer through a systematic approach. Ultrasonic waves originate from thermoelastic expansions, which have been shown to increase through nonradiative heat generation by reduction of reactive oxygen species. Introduction of heavy atoms and halogens can reduce reactive oxygen species generation[30]; therefore, we hypothesize that the inclusion of heavy side chains conjugated to the central squaric acid may enhance non-radiative decay and thermoelastic potential of compounds, leading to increased optoacoustic activity subsequent to excitation. Thus, we undertook a systematic approach to increasing side-chain weight: (1) various halogenation (F, Cl, and Br) at the 5th position of the heterocyclic ring and (2) extended hydrocarbon chains. This study sought to elucidate the potential role of varying the side-chain substitutions at the heterocyclic ring N-atoms in the generation of optoacoustic signals using an *in vivo* model as a first step in identifying the role for specific structural features in generating optoacoustic signals and greater intensities. Further, utilization of computational modeling approaches is hypothesized to develop an understanding of how to optimize optoacoustic contrast agents and potentially provide predictions on the strength of predicted optoacoustic molecules. In addition, a second class of molecules were

synthesized and evaluated for increased optoacoustic signal due to halogenation of side chains. By establishing a foundation of how to optimize an optoacoustic agent, the library of optoacoustic agents will grow, which, in turn, will increase available applications of optoacoustic imaging in a clinical setting.

RESULTS AND DISCUSSION

Dye synthesis and characterization

The identification and development of small molecule dyes that are optimized for optoacoustic imaging is in its preliminary stages. This demands extensive work in designing and synthesizing biosensors with certain structural features that would generate high intensity and unique optoacoustic spectral signals. Optoacoustic probes with tunable features, such as absorption in the near-infrared region (NIR), high extinction coefficient, good photostability, sustained solubility under physiological pH, heavy atoms, and rotatable bonds, requires in-depth design and synthetic approaches. Our lab previously synthesized water-soluble squaraine dyes,

which were highly stable in serum.[31] Due to their improved water solubility and stability in serum, we decided to explore this class of compounds further for their optoacoustic properties. To achieve this goal, we followed the procedure reported by our lab to synthesize the highly stable symmetrical squaraine dyes as shown in Scheme 1. A second class of cyanine compounds (Figure S1) were synthesized subsequently to ensure universal increase of optoacoustic signal due to side-chain halogenation.

We first began the synthesis by performing a Fischer indole cyclization reaction using derivatives of phenyl hydrazine. These non-halogenated (X = H) and halogenated (X = F, Cl, Br) hydrazines were allowed to react with 3-methyl-2-butanone under acidic conditions. The intermediates formed after successfully cyclizing the reactants were further treated with methyl iodide (Mel) or 3-bromo-N, N, N-trimethylpropan-1-ammonium bromide (BrTMAB) in acetonitrile under reflux conditions for 72 h to form salt derivatives, which are intermediates used for synthesis of final squaraines, and were not evaluated. The probe products obtained were cooled down to room temperature and then precipitated out using either acetone or ethyl acetate. The final probes were obtained by reacting the respective indolium salts (2 mol), squaric acid (1 mol), and quinoline in a 50:50 mixture of n-butanol and benzene under reflux conditions for 15 h. To obtain maximum yields, the reactions were done using a Dean Stark apparatus. The reaction mixtures were continuously monitored using vis/NIR spectrophotometry until the dyes' signals were observed. After successful completion of the reactions, the solvents were removed under reduced pressure. The crude products were precipitated using ethyl acetate and acetone and dried under vacuum. The desired optoacoustic squaraine probes were finally obtained following a coprecipitation method using methanol and ethyl acetate. All NMR and mass spectra of the compounds are shown in Figures S2–S16. SQ Br no TMAB is structurally similar to SQ H no TMAB with the substitution of bromine at the X position to determine the effect of bromination without trimethylpropylammonium substitutions.

To determine the photostability of our squaraine derivatives, each compound was incubated in fetal bovine serum (FBS) at 37°C. A stock solution of 1 mM of the squaraine dyes was first prepared in DMSO and an aliquot of these stock solutions (10 μM) was diluted in 100% FBS supplemented with 50 mM HEPES buffer at pH = 7.4, and the absorbance was measured. The working solution was continuously irradiated with a xenon lamp at 150 W for 72 h. The optical responsiveness recognized by their absorbance for each compound tested was measured over the duration of time investigated (Figure 1A). Squaraine dyes (SQ Br and SQ Cl) with bromine and chlorine atoms retained their absorption efficiency over time, leading to consistent optoacoustic signal generation. The photothermal stability exhibited by these dyes influenced how they efficiently dissipate the absorbed energy as heat. A stable squaraine dye is less likely to undergo photodegradation or other chemical changes that could alter its thermal properties. Thus, SQ Br and SQ Cl possess efficient thermal relaxation, which is important for optoacoustic signal generation because it allows these dyes to return to its ground state quickly after absorbing light, leading to repeatable and reliable signal generation. In addition, photodegradable squaraine dye can result in the release of byproducts or changes in the surrounding environment, potentially contributing to background noise in the optoacoustic signal. As a result, photostable squaraine dyes (SQ Br and SQ Cl) are less likely to introduce these sources of noise, enabling clearer and more accurate optoacoustic signal interpretation. Optical and molecular properties of synthesized squaraine are described (Figures 1B and 1C).

Following the synthesis of SQ H no TMAB and SQ H, initial evaluations via MSOT revealed that SQ H exhibited no notable changes in optoacoustic signal intensity when compared with SQ H no TMAB (Figures 2B and 2C). Optoacoustic signal has previously been correlated with number of rotatable bonds in the subject molecule;[25] however, no changes were observed here, likely due to lack of electron-withdrawing moieties in the two compounds. This is supported by the increases in vibrational entropy and oscillator strength associated with the substitution of the methyl group (SQ H no TMAB) with trimethylpropylammonium (SQ H). In addition to optoacoustic data, Figures 2D–2I show the absorbance and fluorescence intensity of each squaraine, and Figure 1B details the optical properties. Notably, the stark difference between fluorescence and absorbance in SQ Br (Figure 2H) suggests the possibility for high optoacoustic activity.

Side chains attached to the heterocyclic terminals are hypothesized to affect vibrational entropy of the molecule and are further investigated here. Addition of various electron-withdrawing or -donating groups can be utilized to maximize photon absorption and provide the molecule with increased size and flexibility for enhanced optoacoustic activity. Because the addition of electronegative atoms increases the electron-withdrawing strength of the heterocyclic terminals, increasingly large halogens were used for side chains in SQ F, SQ Cl, and SQ Br. Similar evaluation via MSOT revealed significant increases in generated optoacoustic signal due to bromine, chlorine, and fluorine substituted side chains in squaraines SQ Br, SQ Cl, and SQ F, respectively (Figures 2A–2C). Following noted increases in SQ Br, SQ H no TMAB was additionally substituted with bromine at the X position without trimethylpropylammonium substitution, resulting in SQ Br no TMAB, which showed increased signal generation. These data suggest that heavy halogen substitutions, combined with the addition of the trimethylpropylammonium group,

may act in tandem to increase optoacoustic activity. The squaraine compounds, when functionalized with halogens, are hypothesized to create suitable energy gaps beneficial for non-radiative energy transfer through dissipation, rather than photon emission. This results in quenching of fluorescence, and amplification of optoacoustic signal.[32] Increasing the weight of the halogen increases the probability of intersystem crossing, further amplifying optoacoustic signal at the expense of fluorescence signal.[33] Results suggest that rotatable bonds from the trimethylpropylammonium group addition are critical for optoacoustic signal.[25,34] Compared with rigid agents, such as rhodamine 800, which contains no rotatable bonds, and displays no optoacoustic activity,[25] squaraine compounds functionalized with trimethylpropylammonium exhibit increased optoacoustic activity. Such structural modifications may be impactful for the development of effective optoacoustic probes.

Quantum mechanical computational modeling

To further understand and identify the variations in experimentally determined optoacoustic capabilities of the trimethylpropylammonium pendant group and halogen substitutions of squaraines, density functional theory (DFT) and timedependent DFT (TD-DFT) were used for a quantum mechanical computational study. DFT and TD-DFT are advanced computational techniques that have been used extensively to gain a deeper understanding of molecular structures and respective absorption and fluorescence properties.[35–38] DFT and TD-DFT calculations were performed using the Q-Chem Software package.[39] For each molecule, the groundstate geometry was optimized in the gas-phase using DFT with the Perdew-BurkeErnzerhof (PBE) functional[40] and 6–31+G* basis set.[41] Cis isomers of squaraine compounds are assumed to be dominant in this context due to similarities in trends of experimental and computational measurements. All computational data for cis isomers are included in the supplemental information (Figures S23–S25; Tables S1–S6). Here, DFT results show a correlation between higher vibrational entropy and MSOT peak intensity between squaraines SQ H no TMAB and SQ H, the sole structural difference being the trimethylpropylammonium in place of the methyl group on SQ H (Figure 3A). Higher vibrational entropies indicate the molecules may have the tendency to undergo interatomic stretching, bending, or rotation more readily, which could enhance non-radiative relaxation channels that generate thermal energy, leading to thermoelastic expansions of higher amplitude and thus optoacoustic signal generation.[42] DFT modeling confirms that squaraines with intense optoacoustic signal have larger vibrational entropies in squaraines with TMAB and halogen substitutions, indicating that maximizing vibrational entropy can enhance optoacoustic signal generation capabilities (Figure 3A).

In general, a greater magnitude of molecular expansion is possible as a result of the halogenated side chains. Maximizing *cis-trans* photo-isomerization is anticipated to contribute to higher dynamics and larger expansion of the molecule, leading to higher optoacoustic intensity (Figures 3D and 3E). This effect may be in part due to the halogens acting as electron-withdrawing groups in the squaraines although the electron-withdrawing strength or halogen electronegativity was found to be inversely correlated to optoacoustic signal intensity. In addition, electronic excitation probability, i.e., oscillator strength, which is directly related to molar absorptivity, of the synthesized molecules trends with

optoacoustic signal strength. As shown in Figure 3B, the oscillator strengths of the relevant absorption peaks from TD-DFT calculations follows the order of Br > Cl > F > H squaraine substitutions, which is in excellent agreement with experimental MSOT observations of squaraines SQ Br > SQ Cl > SQ F > SQ H. Furthermore, SQ H no TMAB was predicted to have the weakest oscillator strength, again, consistent with the weak optoacoustic signal as observed through experimental results.

Computationally, the oscillator strength was obtained as $\frac{2}{3}\Delta E\left|\overrightarrow{\mu}\right|^2$, where ΔE is the absorption energy and $\overrightarrow{\mu}$ is the dipole moment. Figure 3C shows the variation in transition dipole moments among the squaraine compounds, which directly influences the respective predicted oscillator strengths. Similar to the trend in Figure 3B, SQ Br holds the largest transition dipole moment, followed, respectively, by SQ Cl, SQ F, SQ H, SQ BR no TMAB, and SQ H no TMAB. Through these computational studies, we have identified that the trimethylpropylammonium pendant group and the halogen substituents located on the terminal heterocycles are important factors in optimizing optoacoustic signal generation of these compounds.

Figures 4A–4F indicate full computationally derived absorption spectra of squaraines. For MSOT, optoacoustic signal is generated because of the NIR absorption; thus, major and minor peaks at wavelengths below 680 nm do not contribute to optoacoustic signal in a significant fashion. Such peaks in Figure 4 may be disregarded because none has any relation to optoacoustic signal. As expected from experimentally measured optoacoustic activity, a very weak absorption peak is observed around 700 and 752 nm of SQ H no TMAB and SQ Br no TMAB, respectively. In contrast, larger absorption peaks around 700 nm are noted for TMAB-substituted squaraines, each correlating with measured optoacoustic signal (SQ Br > SQ Cl > SQ F > SQ H > SQ H no TMAB). These data suggest that TMAB-functionalized squaraines generate optoacoustic signal after absorption of ~700 nm light, whereas SQ H no TMAB and SQ Br no TMAB weakly absorb ~700/750 nm light and therefore generate minimal optoacoustic signal. SQ H no TMAB, SQ H, SQ F and SQ Br no TMAB exhibited poor thermal stability similarly to the respective optoacoustic activity.

The highest occupied molecular orbital (HOMO) and lowest unoccupied molecular orbital (LUMO) of a compound are regularly used to extract optical and chemical properties, including electron-donating, electron-accepting, stability, and absorbance.[43] Generally, the energy difference between HOMO and LUMO is used to predict strength and stability of the target compound.[44] In this context, frontier orbitals are utilized to explain the significant differences in transition dipole moment in these squaraine compounds with identical conjugation cores. Figure 5 shows the frontier molecular orbitals involved in the electronic excitations that contribute to the absorption peaks of interest where a higher amplitude indicates a larger contribution. Figure 5A shows that the relevant absorption peak for SQ H no TMAB and SQ Br no TMAB are mostly due to an excitation from HOMO-1 (the second HOMO) to LUMO, with an amplitude of 0.9961 and 0.9967, respectively. However, HOMO-1 is localized on the center of the compound, whereas LUMO is fully delocalized over the entire molecule for SQ H no TMAB and SQ Br no TMAB. The

resultant partial charge-transfer character, when combined with the symmetries of HOMO-1 and LUMO orbitals, leads to a near-zero transition dipole moment for SQ H no TMAB and SQ Br no TMAB. For TMAB-substituted squaraines, the charge-transfer character of the first absorption peak was reduced in two ways: (1) contribution to HOMO-1 from trimethylpropylammonium pendant groups caused delocalization of HOMO-1, resulting in a larger degree of overlap between HOMO-1 and LUMO of TMAB-substituted squaraines, and (2) amplitude reduction of HOMO-1 to LUMO excitation compared with SQ H no TMAB and SQ Br no TMAB. Additionally, non-charge-transfer HOMO to LUMO excitation contributed to the absorption peaks of these compounds with amplitudes of 0.4044 (SQ H), 0.4021 (SQ F), 0.4216 (SQ Cl), and 0.4383 (SQ Br), which explains the trend in the predicted transition dipole moments. From this analysis, we hypothesize that changes in electronic excitation character due to trimethylpropylammonium pendant group and halogen substitutions are responsible for varying degrees of photon absorption in the NIR wavelength range, which contributes to the variations in experimentally observed optoacoustic signal intensity (Figure 2B).

Cellular viability

Cells were treated with squaraine dyes of multiple concentrations and evaluated for viability. Although TMAB-substituted squaraines show no toxicity following treatment with cells at both concentrations evaluated, decreases in the viability of cells following treatment with squaraines SQ H no TMAB and SQ Br no TMAB in kidney (Figures 6A and 6E), liver (Figures 6B and 6F), colon (Figures 6C and 6G), and umbilical vein (Figures 6D and 6H) cells. Kidney and liver cells were chosen due to being the major organs involved in clearance of drug injected intravenously.[45] Colon cells were included for consistency with *in vivo* oral gavage administration. Umbilical vein cells were included due to common use as an endothelial cell for *in vitro* studies and because results are often transferable to other endothelial cell types.[46] 200 μg/mL treatment resulted in less viability of cells following the treatment period compared with 20 μg/mL. Minor issues with complete solubility were observed with squaraines SQ H no TMAB and SQ Br no TMAB, which may have contributed to lower viability. However, no treatments imposed any tissue damage, as indicated through histological analysis (Figure 8C). In addition, western blot analysis revealed no changes in caspase-3 protein expression levels compared with untreated cells, indicating the absence of apoptosis as a result of treatment with squaraine dyes (Figure S26). These results indicate that varying alkyl chains can alter charge and salt bridge formation, which contributes to stability and cytotoxicity *in vitro* in addition to vibrational entropy and optoacoustic signal.

In vivo murine model

In vivo comparison of halogen substituted squaraine dyes was determined with MSOT following oral administrations of squaraine dyes into athymic mice. Each animal received 200 μL of dye at 100 μM. Following administration of squaraine compounds, animals were imaged using MSOT. Results corroborate previous *in vitro* results, which indicate SQ Br as the strongest generator of optoacoustic signal (Figures 7A and 7B). Specifically, a mean optoacoustic signal value of 2.12 a.u. was significantly different from all squaraines SQ Cl (0.81 a.u.), SQ F (0.58 a.u.), SQ H (0.44 a.u.), SQ Br no TMAB (0.37 a.u.), and

SQ H no TMAB (0.21 a.u.) ($p < 0.001$, Tukey post hoc). These data support the claim that heavy halogenated squaraine compounds functionalized with the dual TMAB pendant groups generate significantly more optoacoustic activity than counterparts. Evaluation of SQ Br no TMAB follows this trend by exhibiting higher signal than nonhalogenated non-TMAB-functionalized squaraine dye (SQ H no TMAB), but less signal than the TMAB-functionalized squaraine dye with the same bromine substitution (SQ Br). Common optoacoustic contrast agents were evaluated analogously (Figure S27) Following MSOT imaging, animals were imaged using NIR fluorescence, in which similar trends were observed (Figures 7C and 7D). Notably, squaraine SQ Cl showed significantly more NIR fluorescence signal than other squaraines ($p < 0.001$). SQ Br shows potential for future use in a clinical setting, following further mutagenicity and teratogenicity studies. In the context of methods utilized herein, SQ Br could be used as a method to coat the inside of the colon, eliminating the requirement of a barium enema. Because agents given by this administrated method exist the body prior to 6 h (Figure S28), this could aid in the visualization of inflammatory bowel disease through use as a reporter agent specifically for ulcerative colitis or Crohn's disease. This study was designed to exhibit the intensity of a developed reporter dye for optoacoustic imaging. Expanding the collection of optoacoustic dyes will lead to simultaneous imaging of multiple reporter agents, an inherent advantage of MSOT, which has been previously exhibited.[47] Further studies could utilize optoacoustic compounds as a reporter agent through conjugation with a specific targeting molecule for visualization of specific biological processes. In addition, further studies could differ from oral administration of the dye. Oral gavage was chosen specifically to ensure a concentrated focal point *in vivo* for determination and comparison of optoacoustic signal between each of the squaraine compounds. Other administration methods could potentially limit comparisons due to inconsistencies with concentrations in different areas of the animal.

Following *in vivo* evaluation of squaraine compounds, organs were harvested for ex vivo confirmation with NIR fluorescence. Animal colons were imaged using NIR fluorescence to confirm squaraine presence in the colon (Figures 8A, 8B, and S29). Squaraine compounds were confirmed to be in the stool of the animal through NIR fluorescence imaging after washing of the colon with saline (Figure S30). Squaraines were confirmed to be absent from the kidney, liver, and spleen (Figures 8A and 8B).

Histological evaluation of the colon, liver, kidney, and spleen by a board-certified pathologist following *in vivo* administration was performed to ensure that treatments with squaraine compounds were non-toxic to the evaluated animals. Assessment of histology showed little morphological changes outside the usual, indicating no treatment-imposed tissue damage (Figure 8C). In combination with lack of cellular toxicity (Figure 6), TMAB-substituted halogenated squaraine dyes give no indication of toxicity.

Halogenated cyanine dyes

To ensure that changes in halogenation are not limited to squaraine molecules,an additional set of cyanine dyes were synthesized according to information derived from halogenated squaraines, coined as CY H, CY Cl, and CY Br (Figure S1 and Figures S17–S22). Notably, *in vitro* evaluation of CY dyes corroborated results from squaraine analogs; bromination

(CY Br) resulting in the largest increase in optoacoustic activity, followed by chlorination (CY Cl), with non-halogenated counterpart (CY H) exhibiting the least optoacoustic signal (Figure S31). In addition, full DFT/TD-DFT calculations were performed to ensure trends in vibrational entropy, oscillator strength, and transition dipole moment were consistent with heavy halogenation (Figures S32–S39; Tables S7–S9). Although CY dyes show significantly lower optoacoustic relevant oscillator strengths, the trends were constant with squaraine compounds, with the largest strengths observed in the bromine substituted CY Br, compared with chlorine substituted CY Cl, and non-halogenated CY H. Cell viability (FigureS40) and photostability (Figure S41) studies were performed prior to *in vivo* studies to ensure non-toxicity for oral administration. *In vivo* evaluation of CY dyes confirmed *in vitro* studies and corroborate information from squaraine compounds. CY Br showed the highest optoacoustic signal *in vivo* (1.12 a.u.), followed by CY Cl (0.70 a.u.), and the least signal from CY H (0.25 a.u.), indicating the trend of bromination > chlorination > non-halogenation (Figure S42). Fluorescence whole-body animal imaging and ex vivo imaging was performed consistent with previous squaraine studies (Figure S42). These data suggest that heavy halogenation for the purposes of increasing optoacoustic intensity is a universal property that may be utilized in the development of optoacoustic contrast agents.

Limitations of the study

The purpose of this study focused on the evaluation of how structural moieties alter the optoacoustic signal generation of a set of squaraine dyes. The squaraines utilized in this study were chosen for the purpose of practicality because the simple synthesis and backbone of the squaraines limit confounding factors that would be present in complex molecules. However, more complex and asymmetric molecules could be utilized to provide a more nuanced understanding based on the exact set of dyes. Although a second set of cyanine dyes were evaluated in this study (supplemental information) and confirmed to share the relationship between heavy halogenation and optoacoustic signal increases, this study does not necessitate heavy halogenation for strong optoacoustic contrast agents. Due to the multiple variables that could cause changes in optoacoustic signal, factors such as substitution at different position and alterations of the TMAB chain length were unable to be evaluated in tandem with heavy halogenation and TMAB substitution. However, through the computational modeling and results, predictions of the optoacoustic signal strength may be implied through molecular structure prior to compound synthesis in the future.

This work had a focus on utilizing squaraine dyes modified with trimethylpropylammonium and halogen atoms for an emerging, clinically relevant optoacoustic imaging modality, MSOT. As previously mentioned, MSOT is a rapidly developing modality that has proven efficacy in clinical trials due to intrinsic advantages over traditional imaging techniques. With a current lack of guidelines for developing optimized optoacoustic contrast agents, the purpose of this study was to investigate how variations in squaraine dyes affect optoacoustic signal generation. That is, the purpose of this manuscript was to establish how substitutions to the molecular structure of squaraine dyes impacted the resultant optoacoustic signal generation, a relationship that is currently poorly understood. Replacement of a methyl group with a trimethylpropylammonium pendant group resulted in significant increases in optoacoustic signal due to increased rotational bonds and vibrational entropy. Using

DFT/TD-DFT increases in the oscillatory strength was attributed to larger transition dipole moments arising from varied frontier orbital character. *In vivo* analysis of a mouse model corroborated observations that heavy halogen squaraine compounds with dual trimethylpropylammonium groups resulted in high-resolution optoacoustic imaging. In addition, a second compound class (CY) was synthesized to ensure utilization of heavy halogenation to boost optoacoustic signal is a universal property. Although this study utilized oral gavage as the method of administration of contrast agent to ensure equally as strong concentrated areas of compounds *in vivo*, this is different than application in a clinical setting. Further developments of squaraines, as well as other contrast agents will continue to increase the relevance and value of MSOT in a clinical setting; through spectral unmixing, several different contrast agents can be differentiated based on spectral signature.[47,48]

EXPERIMENTAL PROCEDURES

Resource availability

Lead contact—Further information and requests for resources should be directed to and will be fulfilled by the lead contact, Lacey McNally (lacey_mcnally@hotmail.com).

Materials availability—All unique reagents generated in this study are available from Dr. Maged Henary (mhenary1@gsu.edu).

Supplementary Material

Refer to Web version on PubMed Central for supplementary material.

ACKNOWLEDGMENTS

We acknowledge funding from the National Institutes of Health under grants F31CA261044, R01CA205941, R01EB034731, R01CA281098, R01GM135392, and P30CA225520.

Data and code availability

This study did not generate any datasets.

REFERENCES

1. MacCuaig WM, Jones MA, Abeyakoon O, and McNally LR (2020). Development of multispectral optoacoustic tomography as a clinically translatable modality for cancer imaging. Radiol. Imaging Cancer 2, e200066.
2. McNally LR, Mezera M, Morgan DE, Frederick PJ, Yang ES, Eltoum IE, and Grizzle WE (2016). Current and emerging clinical applications of multispectral optoacoustic tomography (MSOT) in oncology. Clin. Cancer Res. 22, 3432–3439. [PubMed: 27208064]
3. Wang LV, and Hu S. (2012). Photoacoustic tomography: in vivo imaging from organelles to organs. Science 335, 1458–1462. [PubMed: 22442475]
4. Samykutty A, Grizzle WE, Fouts BL, McNally MW, Chuong P, Thomas A, Chiba A, Otali D, Woloszynska A, Said N, et al. (2018). Optoacoustic imaging identifies ovarian cancer using a microenvironment targeted theranostic wormhole mesoporous silica nanoparticle. Biomaterials 182, 114–126. [PubMed: 30118979]

5. Attia ABE, Balasundaram G, Moothanchery M, Dinish US, Bi R, Ntziachristos V, and Olivo M. (2019). A review of clinical photoacoustic imaging: current and future trends. Photoacoustics 16, 100144.
6. Han Z, MacCuaig WM, Gurcan MN, Claros-Sorto J, Garwe T, Henson C, Holter-Chakrabarty J, Hannafon B, Chandra V, Wellberg E, et al. (2023). Dynamic 2-deoxy-D-glucose-enhanced multispectral optoacoustic tomography for assessing metabolism and vascular hemodynamics of breast cancer. Photoacoustics 32, 100531.
7. Regensburger AP, Wagner AL, Claussen J, Waldner MJ, and Knieling F. (2020). Shedding light on pediatric diseases: multispectral optoacoustic tomography at the doorway to clinical applications. Mol. Cell. Pediatr. 7, 3. [PubMed: 32130546]
8. Regensburger AP, Brown E, Krönke G, Waldner MJ, and Knieling F. (2021). Optoacoustic imaging in inflammation. Biomedicines 9, 483. [PubMed: 33924983]
9. Manohar S, and Gambhir SS (2020). Clinical photoacoustic imaging. Photoacoustics 19, 100196.
10. Regensburger AP, Fonteyne LM, Jüngert J, Wagner AL, Gerhalter T, Nagel AM, Heiss R, Flenkenthaler F, Qurashi M, Neurath MF, et al. (2019). Detection of collagens by multispectral optoacoustic tomography as an imaging biomarker for Duchenne muscular dystrophy. Nat. Med. 25, 1905–1915. [PubMed: 31792454]
11. Zhang HF, Maslov K, Sivaramakrishnan M, Stoica G, and Wang LV (2007). Imaging of hemoglobin oxygen saturation variations in single vessels in vivo using photoacoustic microscopy. Appl. Phys. Lett. 90, 53901.
12. Upputuri PK, and Pramanik M. (2020). Recent advances in photoacoustic contrast agents for in vivo imaging. Wiley Interdiscip. Rev. Nanomed. Nanobiotechnol. 12, e1618. [PubMed: 32027784]
13. Diot G, Metz S, Noske A, Liapis E, Schroeder B, Ovsepian SV, Meier R, Rummeny E, and Ntziachristos V. (2017). Multispectral optoacoustic tomography (MSOT) of human breast cancer. Clin. Cancer Res. 23, 6912–6922. [PubMed: 28899968]
14. Neuschler EI, Butler R, Young CA, Barke LD, Bertrand ML, Bö hm-Vé lez M, Destounis S, Donlan P, Grobmyer SR, Katzen J, et al. (2018). A pivotal study of optoacoustic imaging to diagnose benign and malignant breast masses: a new evaluation tool for radiologists. Radiology 287, 398–412. [PubMed: 29178816]
15. Becker A, Masthoff M, Claussen J, Ford SJ, Roll W, Burg M, Barth PJ, Heindel W, Schäfers M, Eisenblätter, M., et al. (2018). Multispectral optoacoustic tomography of the human breast: characterisation of healthy tissue and malignant lesions using a hybrid ultrasound-optoacoustic approach. Eur. RadIOL. 28, 602–609. [PubMed: 28786007]
16. Knieling F, Hartmann A, Uter W, Urich A, Claussen J, Atreya R, Rascher W, and Waldner M. (2017). Multispectral optoacoustic tomography in Crohn's disease - a first-in-human diagnostic clinical trial. J. Nucl. Med. 58, 379–386. [PubMed: 27609788]
17. Knieling F, Hartmann A, Claussen J, Urich A, Atreya R, Rascher W, and Waldner M. (2017). Multispectral optoacoustic tomography in ulcerative colitis - first-in-human diagnostic clinical trial. J. Nucl. Med. 58, 1196–1200. [PubMed: 28663195]
18. Knieling F, Neufert C, Hartmann A, Claussen J, Urich A, Egger C, Vetter M, Fischer S, Pfeifer L, Hagel A, et al. (2017). Multispectral optoacoustic tomography for assessment of Crohn's disease activity. N. Engl. J. Med. 376, 1292–1294. [PubMed: 28355498]
19. Attia ABE, Chuah SY, Razansky D, Ho CJH, Malempati P, Dinish US, Bi R, Fu CY, Ford SJ, Lee JS-S, et al. (2017). Noninvasive real-time characterization of nonmelanoma skin cancers with handheld optoacoustic probes. Photoacoustics 7, 20–26. [PubMed: 28652976]
20. Masthoff M, Helfen A, Claussen J, Roll W, Karlas A, Becker H, Gabriëls GRiess JHeindel WSchäfers Met al. (2018). Multispectral optoacoustic tomography of systemic sclerosis. J. Biophotonics 11, e201800155.
21. Joseph J, Tomaszewski MR, Quiros-Gonzalez I, Weber J, Brunker J, and Bohndiek SE (2017). Evaluation of precision in optoacoustic tomography for preclinical imaging in living subjects. J. Nucl. Med. 58, 807–814. [PubMed: 28126890]
22. Zhang Y, He S, Chen W, Liu Y, Zhang X, Miao Q, and Pu K. (2021). Activatable polymeric nanoprobe for near-infrared fluorescence and photoacoustic imaging of T lymphocytes. Angew. Chem. Int. Ed. Engl. 133, 5986–5992.

23. Shao Q, and Ashkenazi S. (2015). Photoacoustic lifetime imaging for direct in vivo tissue oxygen monitoring. J. Biomed. Opt. 20, 36004.
24. Beziere N, Lozano N, Nunes A, Salichs J, Queiros D, Kostarelos K, and Ntziachristos V. (2015). Dynamic imaging of PEGylated indocyanine green (ICG) liposomes within the tumor microenvironment using multi-spectral optoacoustic tomography (MSOT). Biomaterials 37, 415–424. [PubMed: 25453969]
25. Laramie MD, Smith MK, Marmarchi F, McNally LR, and Henary M. (2018). Small molecule optoacoustic contrast agents: an unexplored avenue for enhancing in vivo imaging. Molecules 23, 2766. [PubMed: 30366395]
26. Song KH, Stein EW, Margenthaler JA, and Wang LV (2008). Noninvasive photoacoustic identification of sentinel lymph nodes containing methylene blue in vivo in a rat model. J. Biomed. Opt. 13, 54033.
27. Chen J, Liu C, Zeng G, You Y, Wang H, Gong X, Zheng R, Kim J, Kim C, and Song L. (2016). Indocyanine green loaded reduced graphene oxide for in vivo photoacoustic/fluorescence dual-modality tumor imaging. Nanoscale Res. Lett. 11, 85. [PubMed: 26868422]
28. Li W, Peng J, Yang Q, Chen L, Zhang L, Chen X, and Qian Z. (2018). α-Lipoic acid stabilized DTX/IR780 micelles for photoacoustic/fluorescence imaging guided photothermal therapy/chemotherapy of breast cancer. Biomater. Sci. 6, 1201–1216. [PubMed: 29578215]
29. Ilina K, MacCuaig WM, Laramie M, Jeouty JN, McNally LR, and Henary M. (2020). Squaraine dyes: molecular design for different applications and remaining challenges. Bioconjug. Chem. 31, 194–213. [PubMed: 31365819]
30. Weng XL, and Liu JY (2021). Strategies for maximizing photothermal conversion efficiency based on organic dyes. Drug Discov. Today 26, 2045–2052. [PubMed: 33741495]
31. Yadav Y, Owens E, Nomura S, Fukuda T, Baek Y, Kashiwagi S, Choi HS, and Henary M. (2020). Ultrabright and serum-stable squaraine dyes. J. Med. Chem. 63, 9436–9445. [PubMed: 32787096]
32. Liu Y, Teng L, Yin B, Meng H, Yin X, Huan S, Song G, and Zhang XB (2022). Chemical design of activatable photoacoustic probes for precise biomedical applications. Chem. Rev. 122, 6850–6918. [PubMed: 35234464]
33. Koziar JC, and Cowan DO (1978). Photochemical heavy-atom effects. Acc. Chem. Res. 11, 334–341.
34. St Lorenz A, Buabeng ER, Taratula O, Taratula O, and Henary M. (2021). Nearinfrared heptamethine cyanine dyes for nanoparticle-based photoacoustic imaging and photothermal therapy. J. Med. Chem. 64, 8798–8805. [PubMed: 34081463]
35. Al-Otaibi JS, and Al-Wabli RI (2015). Vibrational spectroscopic investigation (FT-IR and FT-Raman) using ab initio (HF) and DFT (B3LYP) calculations of 3-ethoxymethyl-1,4-dihydroquinolin-4-one. Spectrochim. Acta A Mol. Biomol. Spectrosc. 137, 7–15. [PubMed: 25180666]
36. An X-X, Liu C, Chen Z-Z, Xie K-F, and Zhang Y. (2019). Fluorescence properties and density functional theory calculation of a structurally characterized heterotetranuclear [ZnII2–SmIII2] 4,4′-bipy-salamo-constructed complex. Crystals 9, 602.
37. Essam ZM, Ozmen GE, Setiawan D, Hamid RR, Abd El-Aal RM, Aneja R, Hamelberg D, and Henary M. (2021). Donor acceptor fluorophores: synthesis, optical properties, TD-DFT and cytotoxicity studies. Org. Biomol. Chem. 19, 1835–1846. [PubMed: 33565564]
38. Furche F, and Ahlrichs R. (2002). Adiabatic time-dependent density functional methods for excited state properties. J. Chem. Phys. 117, 7433–7447.
39. Epifanovsky E, Gilbert ATB, Feng X, Lee J, Mao Y, Mardirossian N, Pokhilko P, White AF, Coons MP, Dempwolff AL, et al. (2021). Software for the frontiers of quantum chemistry: an overview of developments in the Q-Chem 5 package. J. Chem. Phys. 155, 84801.
40. Perdew JP, Burke K, and Ernzerhof M. (1996). Generalized gradient approximation made simple. Phys. Rev. Lett. 77, 3865–3868. [PubMed: 10062328]
41. Hehre WJ, Ditchfield R, and Pople JA (1972). Self—consistent molecular orbital methods. XII. Further extensions of Gaussian—type basis sets for use in molecular orbital studies of organic molecules. J. Chem. Phys. 56, 2257–2261.

42. Gao F, Kishor R, Feng X, Liu S, Ding R, Zhang R, and Zheng Y. (2017). An analytical study of photoacoustic and thermoacoustic generation efficiency towards contrast agent and film design optimization. Photoacoustics 7, 1–11. [PubMed: 28603690]

43. Roncali J. (2007). Molecular engineering of the band gap of π-conjugated systems: facing technological applications. Macromol. Rapid Commun. 28, 1761–1775.

44. Yanagisawa S, Yasuda T, Inagaki K, Morikawa Y, Manseki K, and Yanagida S. (2013). Intermolecular interaction as the origin of red shifts in absorption spectra of zincphthalocyanine from first-principles. J. Phys. Chem. A 117, 11246–11253. [PubMed: 24106753]

45. Toutain PL, and Bousquet-Mélou, A. (2004). Plasma clearance. J. Vet. Pharmacol. Ther. 27, 415–425. [PubMed: 15601437]

46. Lau S, Gossen M, Lendlein A, and Jung F. (2021). Venous and arterial endothelial cells from human umbilical cords: potential cell sources for cardiovascular research. Int. J. Mol. Sci. 22, 978. [PubMed: 33478148]

47. Zeiderman MR, Morgan DE, Christein JD, Grizzle WE, McMasters KM, and McNally LR (2016). Acidic pH-targeted chitosan capped mesoporous silica coated gold nanorods facilitate detection of pancreatic tumors via multispectral optoacoustic tomography. ACS Biomater. Sci. Eng. 2, 1108–1120. [PubMed: 28626793]

48. Laramie MD, Fouts BL, MacCuaig WM, Buabeng E, Jones MA, Mukherjee P, Behkam B, McNally LR, and Henary M. (2021). Improved pentamethine cyanine nanosensors for optoacoustic imaging of pancreatic cancer. Sci. Rep. 11, 4366. [PubMed: 33623069]

Highlights

- Non-toxic, near-infrared squaraine dyes synthesized for optoacoustic imaging
- Computational modeling used to predict optoacoustic signal intensity
- Heavy halogenation and rotatable bonds improved optoacoustic signal strength
- Strong optoacoustic signal was visualized in mice administered with squaraines

THE BIGGER PICTURE

The role of structural features and their influence on the generation of optoacoustic signal remains an area of limited exploration. This work begins the development of a framework that is expected to be followed with subsequent evaluations to deepen the understanding of how to develop and optimize optoacoustic imaging agents. This framework is necessary to our understanding to effectively create a library of unique optoacoustic agents. This information has implications in diagnostics; following contrast agent understanding and development, advancement and specification will follow. Thus, the utilization of optimized optoacoustic imaging will provide quality anatomical and biological process information in a clinical setting. Contrast-based optoacoustic imaging has the potential to impact disease monitoring and progression as a single or co-modality, which have been supported by previous, nontargeted contrast clinical trials.

A

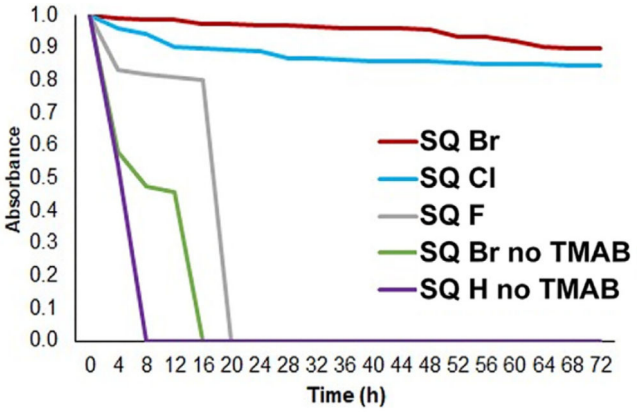

B

Molecule	Λ_{abs} (nm)	Λ_{ems} (nm)	Extinction Coefficient ($M^{-1}cm^{-1}$)	Quantum Yield (Φ, %)	Optoacoustic Mean Intensity ($x10^{-2}$) (a.u.)
SQ H no TMAB	624	629	129,777	37	0.37
SQ H	630	645	168,350	-	0.38
SQ F	637	646	193,950	40	0.58
SQ Cl	638	656	229,800	40	4.20
SQ Br	638	656	204,000	28	5.70
SQ Br no TMAB	634	639	109,324	30	1.65

C

Molecule	Rotatable Bonds	Surface Area ($Å^2$)	Volume ($Å^3$)	LogD
SQ H no TMAB	8	550	403	-1.2
SQ H	20	796	594	-5.1
SQ F	20	813	607	-4.8
SQ Cl	20	809	622	-3.9
SQ Br	20	818	635	-3.5
SQ Br no TMAB	8	569	443	0.1

Figure 1. Photothermal, optical, and molecular properties of squaraine compounds

(A) Photothermal stability of squaraines. Compounds were diluted to an optical absorbance of 1 and re-measured after irradiation with a UV lamp.

(B) Optical properties for squaraines in FBS supplemented with HEPES buffer at pH 7.4 and warmedto physiological temperature 37 °C).

(C) Molecular properties of squaraines. Rotatable bonds, surface area, and volume were computedwith RDkit. LogD (pH 7.4) was computed with ChemAxon.

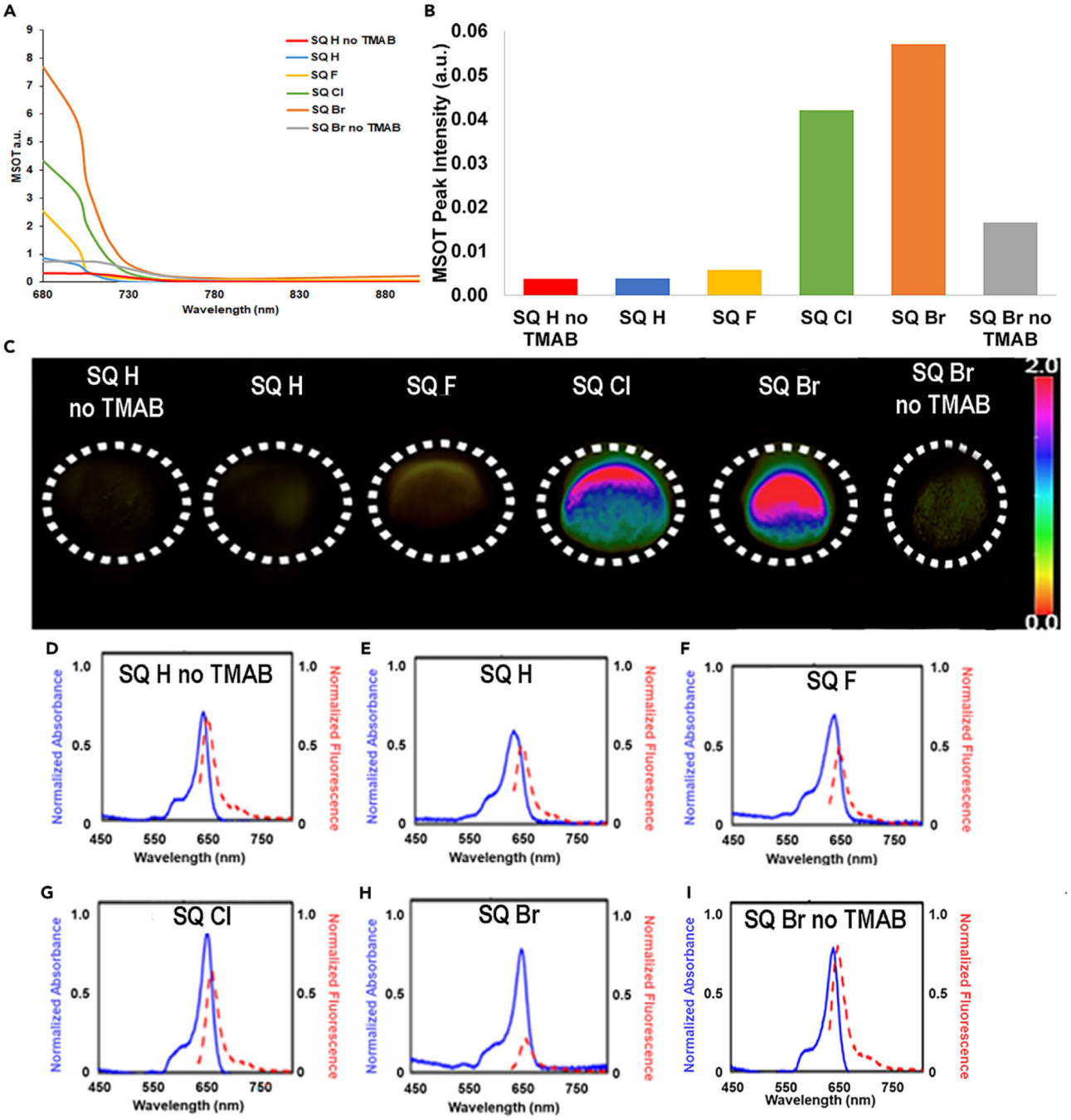

Figure 2. Optoacoustic evaluation of squaraines

(A) Absorption spectra of notable squaraines.

(B) Peak optoacoustic intensity of squaraines.

(C) Optoacoustic images of squaraines in tissue-mimicking phantoms.

(D) Absorption (10 μM) and fluorescence spectra (2 μM) for SQ H no TMAB*.

(E) Absorption (10 μM) and fluorescence spectra (2 μM) for SQ H*.

(F) Absorption (10 μM) and fluorescence spectra (2 μM) for SQ F*.

(G) Absorption (10 μM) and fluorescence spectra (2 μM) for SQ Cl*.

(H) Absorption (10 μM) and fluorescence spectra (2 μM) for SQ Br*.
(I) Absorption (10 μM) and fluorescence spectra (2 μM) for SQ Br no TMAB8.
*Absorption and fluorescence spectra measured in 100% FBS supplemented with 50 mM HEPES buffer at pH = 7.4 and warmed to physiological temperature (37 °C).

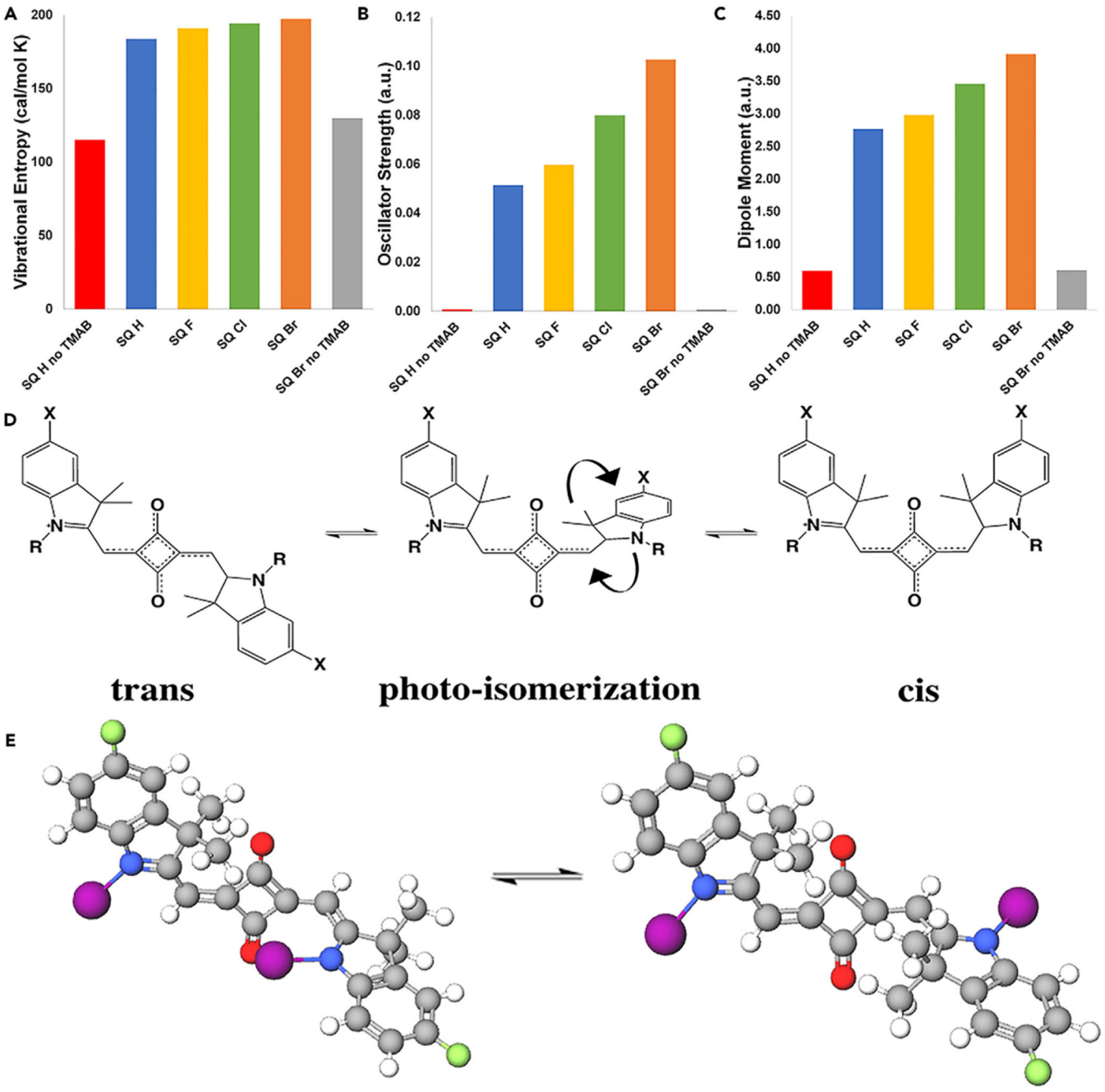

Figure 3. Computational modeling of squaraines

(A) Vibrational entropy of squaraines from DFT frequency calculations*.

(B) Oscillator strength of the lowest energy absorptions of squaraines in cis conformations from TD-DFT calculations*.

(C) Transition dipole moment of the lowest energy absorptions of squaraines in cis conformations from TD-DFT calculations*.

(D) 2D structure of squaraines in *trans* and *cis* conformations through photo-isomerization.

(E) 3D structure of squaraines in *trans* and *cis* formations through photo-isomerization.

PBE functional and 6–31+G basis set were used in all DFT and TD-DFT calculations.

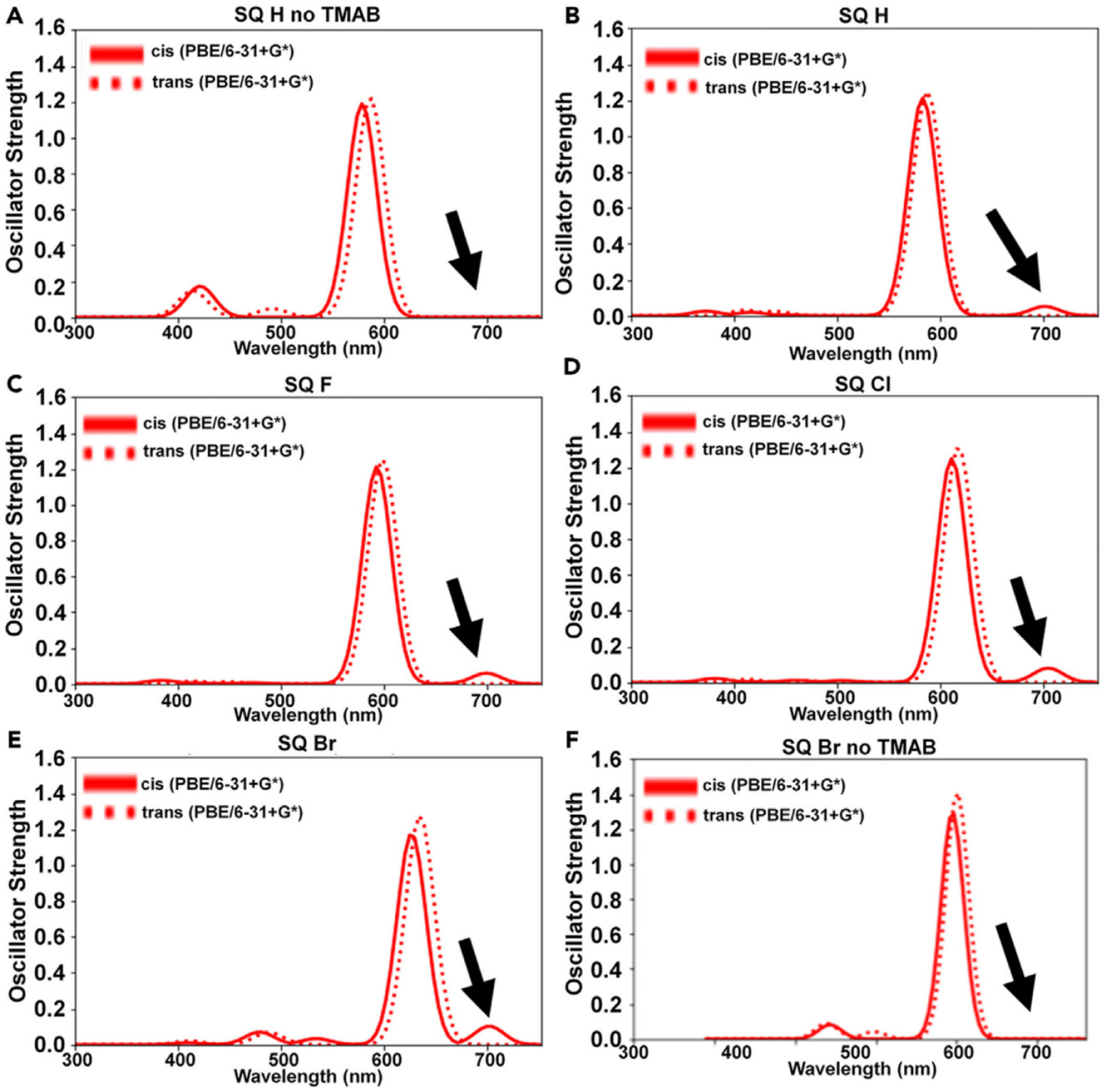

Figure 4. TD-DFT derived absorption peaks of cis and trans isomers of squaraine compounds

(A) TD-DFT-derived absorption peaks for isomers of SQ H no TMAB.

(B) TD-DFT-derived absorption peaks for isomers of SQ H.

(C) TD-DFT-derived absorption peaks for isomers of SQ F.

(D) TD-DFT-derived absorption peaks for isomers of SQ Cl.

(E) TD-DFT-derived absorption peaks for isomers of SQ Br.

(F) TD-DFT-derived absorption peaks for isomers of SQ Br no TMAB.

*Arrows in (A)–(F) indicate the absorption peak that is responsible for optoacoustic signal generation.

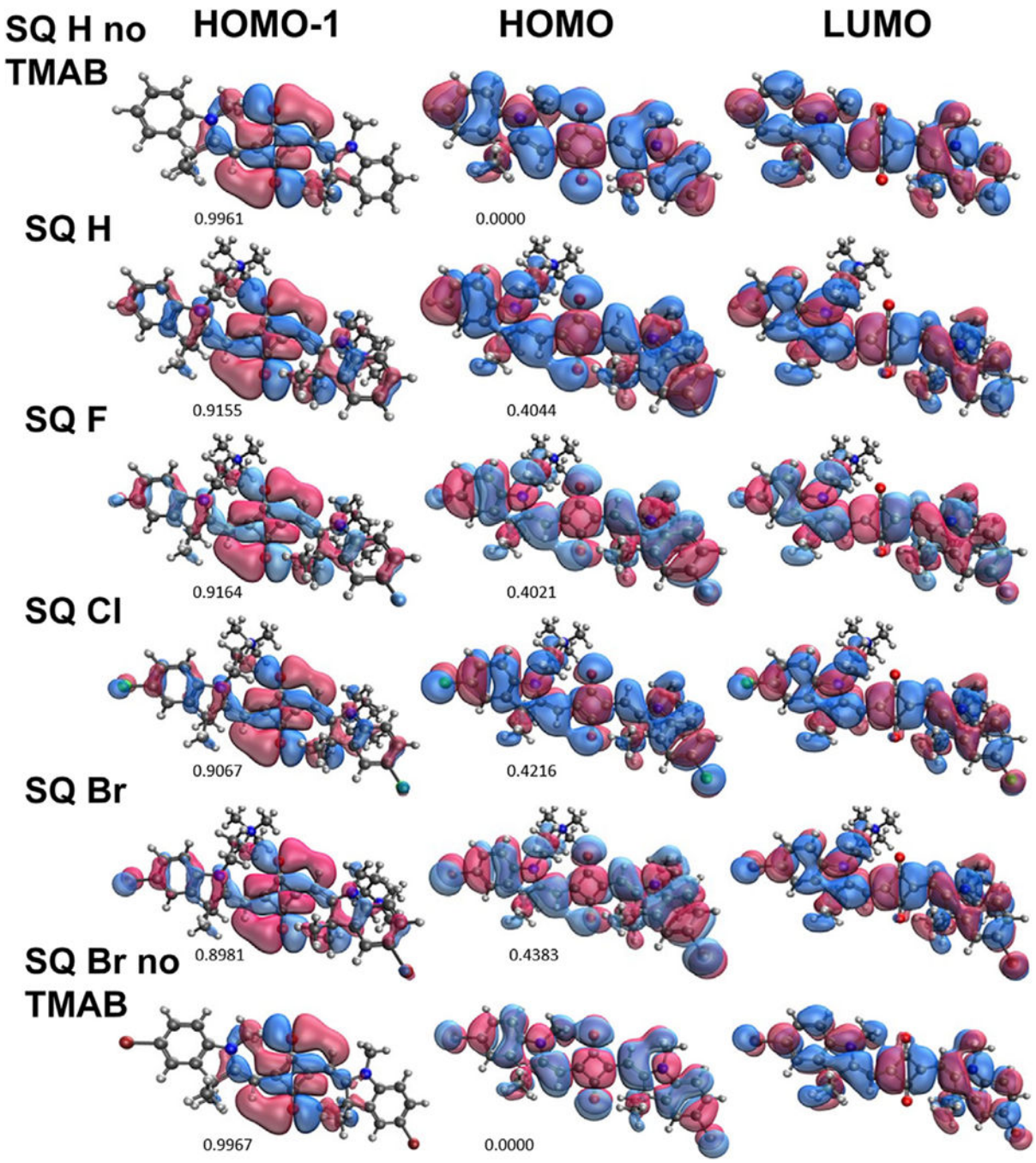

Figure 5. Orbital energy maps of squaraines

HOMO-1, HOMO, and LUMO energy maps of squaraines from DFT calculations using PBE functional and 6–31+G* basis set. Amplitudes for HOMO-1 to LUMO and HOMO to LUMO electronic transitions for the lowest energy absorption are listed below the respective orbitals. For a specific molecular orbital (HOMO-1, HOMO, or LUMO), isosurfaces are shown in blue (isovalue = 0.02) and red (isovalue = −0.02).

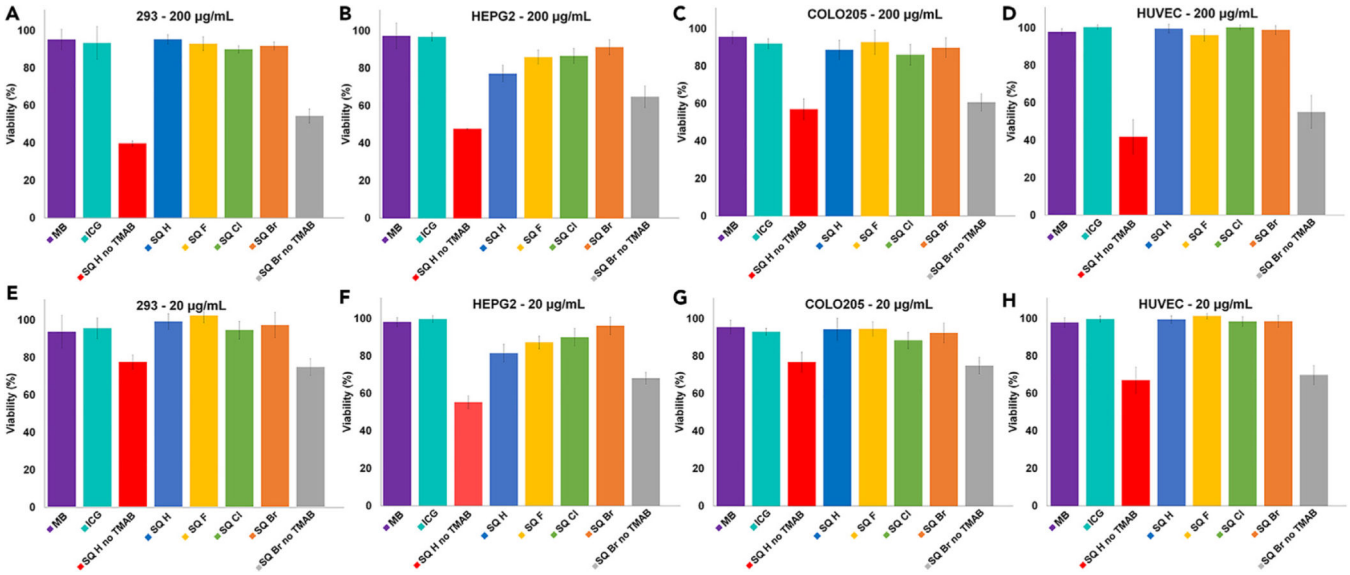

Figure 6. Cellular viability of cells following treatment with squaraines

(A) 293 kidney cells at 200 µg/mL squaraine treatment.

(B) HEPG2 liver cells at 200 µg/mL squaraine treatment.

(C) COLO205 colon cells at 200 µg/mL squaraine treatment.

(D) HUVEC umbilical vein endothelial cells at 200 µg/mL squaraine treatment.

(E) 293 kidney cells at 20 µg/mL squaraine treatment.

(F) HEPG2 liver cells at 20 µg/mL squaraine treatment.

(G) COLO205 colon cells at 20 µg/mL squaraine treatment.

(H) HUVEC umbilical vein endothelial cells at 20 mg/mL squaraine treatment. Error bars represent ± 1 standard deviation.

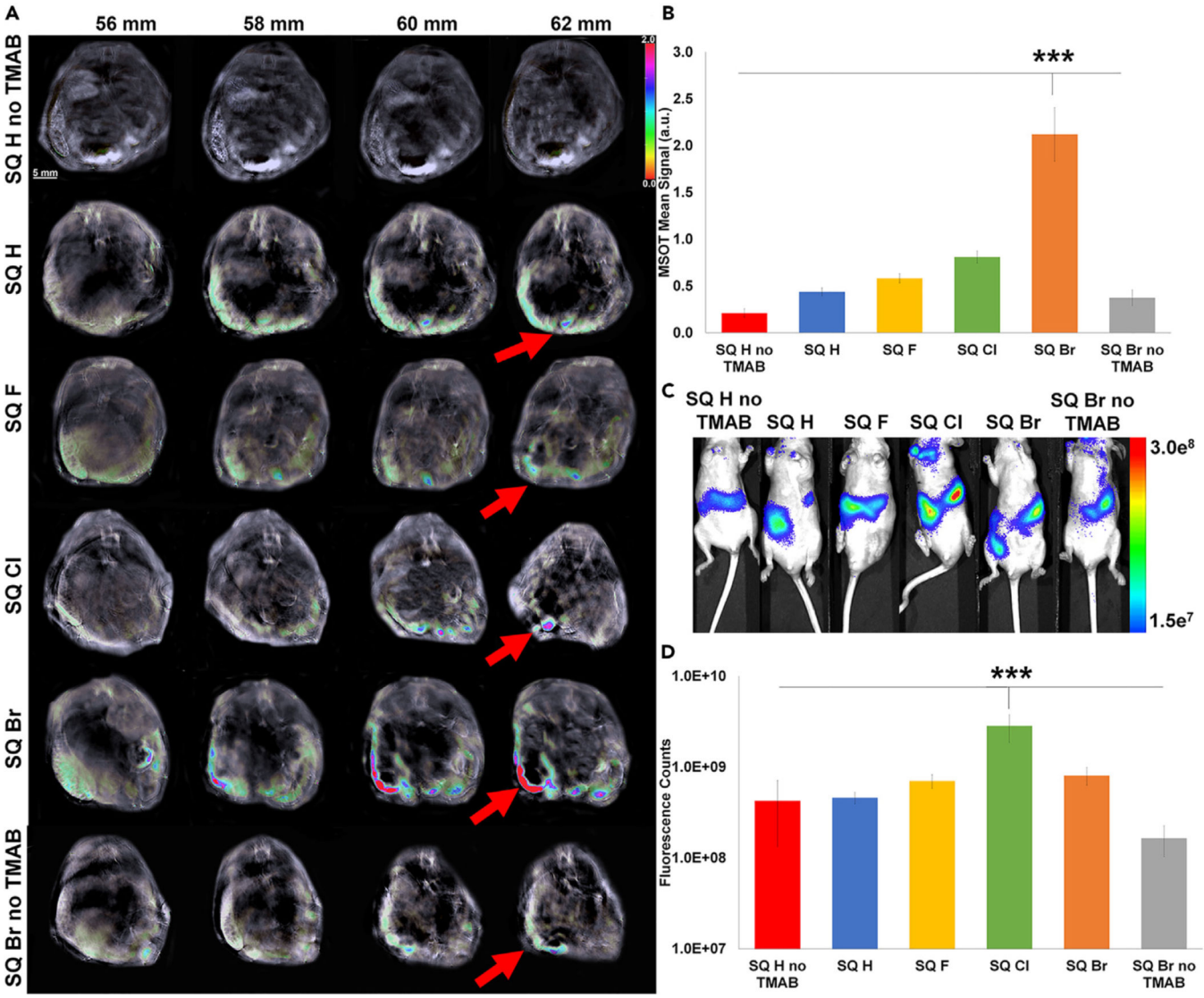

Figure 7. *In vivo* visualization of squaraine compounds

(A) *In vivo* visualization of optoacoustic signal generated from squaraines subsequent to oral administration. Columns represent slightly different tomographic slices within the mouse. Red arrows show optoacoustic signal as a result of squaraine compounds in the colon.

(B) Quantification of optoacoustic signal observed in (A) (n = 3).

(C) *In vivo* visualization of NIR fluorescence signal generated from squaraines.

(D) Quantification of NIR fluorescence signal observed in (C). *p < 0.08, **p < 0.01, ***p < 0.001. Error bars represent ± 1 standard deviation.

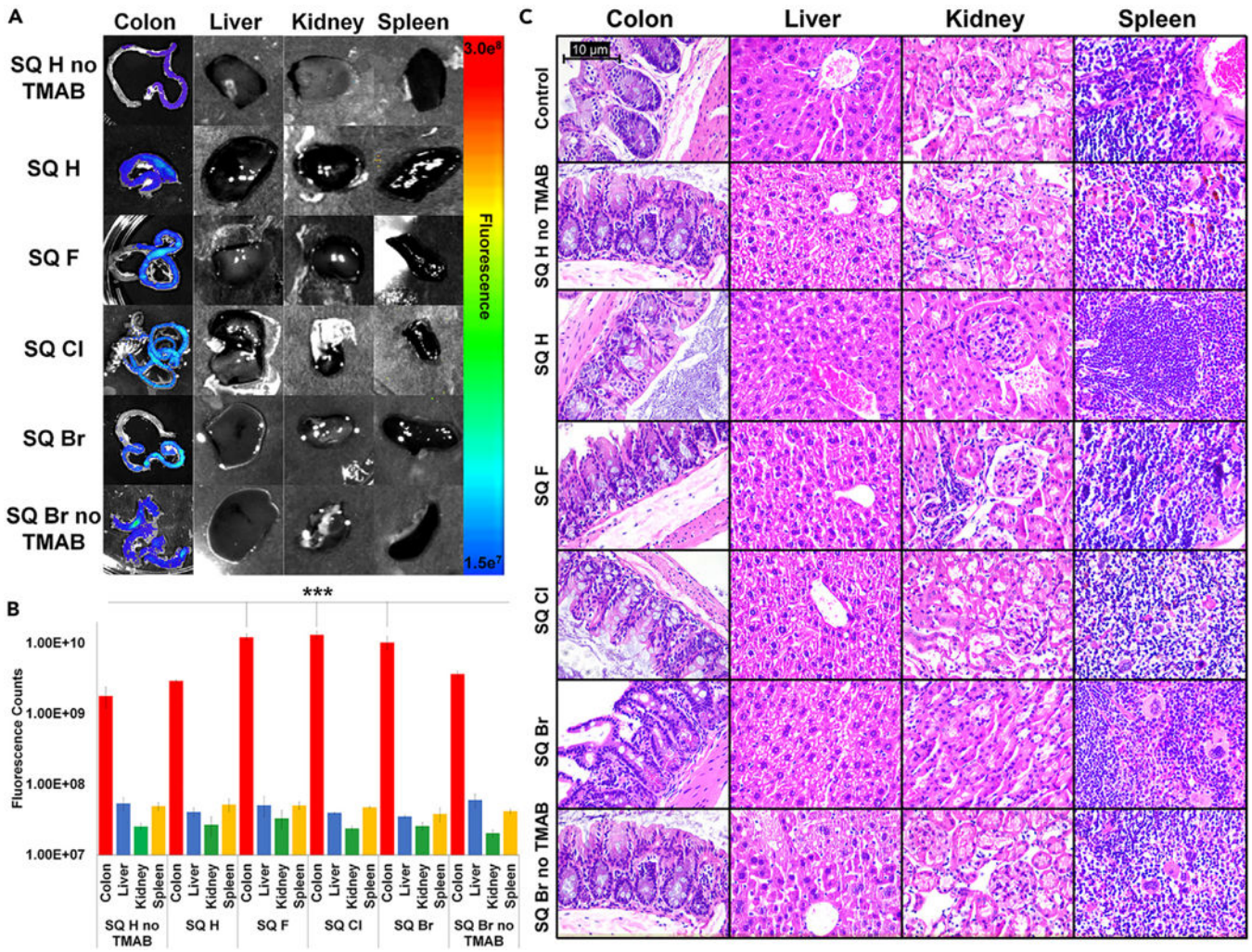

Figure 8. Ex vivo confirmation of squaraine presence and non-toxicity

(A) Ex vivo visualization of NIR fluorescence signal generated from squaraine compounds in animal colons, livers, spleens, and kidneys subsequent to oral administration.

(B) Quantification of NIR fluorescence signal observed in (A).

(C) H&E histology images of colon, liver, kidney, and spleen of animals treated with squaraine compounds. Images show no unusual morphology, indicating little risk of squaraine treatment on organs. *$p < 0.08$, **$p < 0.01$, ***$p < 0.001$. Error bars represent ± 1 standard deviation.

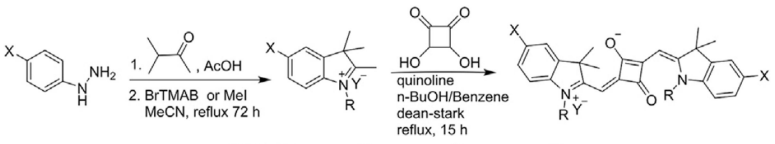

R1 = Me
R2 = TMAB
X1 = H
X2 = F
X3 = Cl
X4 = Br

Molecule	R	X	Y
SQ H no TMAB	Me	H	I
SQ H	TMAB	H	Br
SQ F	TMAB	F	Br
SQ Cl	TMAB	Cl	Br
SQ Br	TMAB	Br	Br
SQ Br no TMAB	Me	Br	I

Scheme 1. Synthetic route for squaraine optoacoustic probes